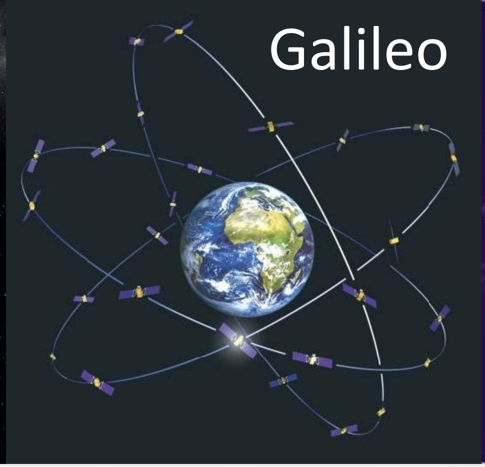

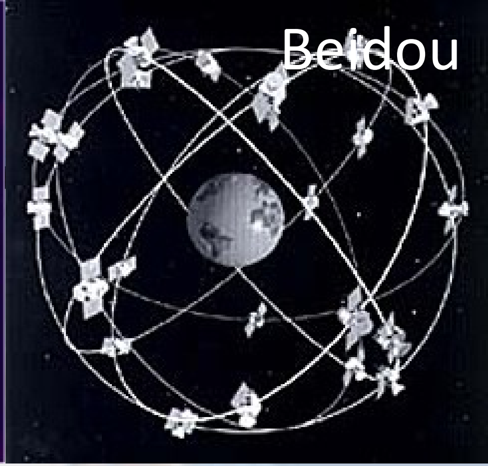

GNSS remote sensing (GNSS-RS)

Shuanggen Jin（金双根）
Shanghai Astronomical Observatory, CAS, Shanghai 200030, China
Email: sgjin@shao.ac.cn
Website: http://www.shao.ac.cn/geodesy

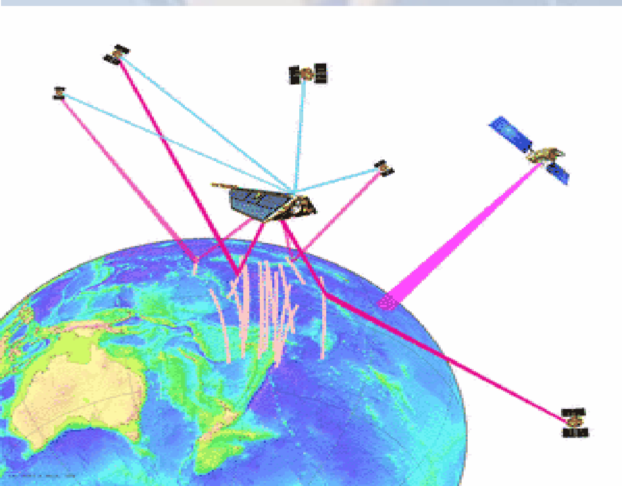
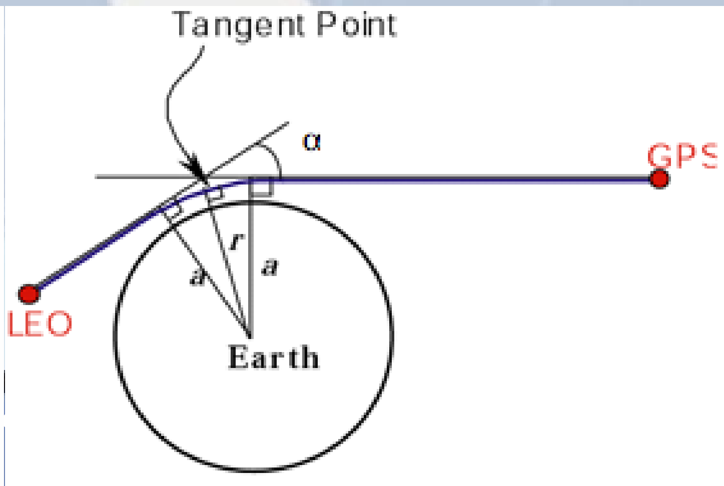

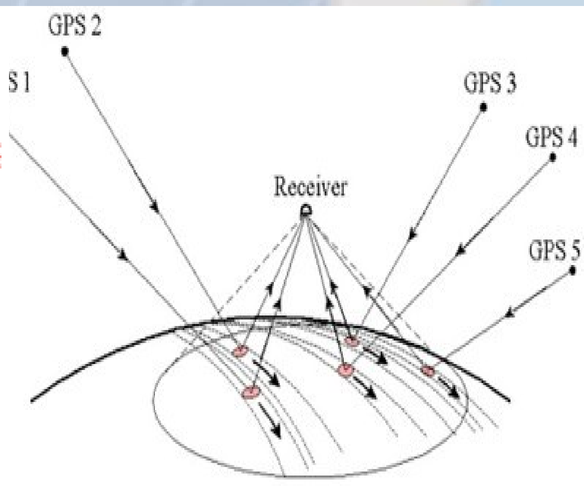

Outline

- Introduction
- GNSS remote sensing
- GNSS-RS Current Status
- Future Development

GNSS

(GPS, GLANNAS, Galileo and Compass)

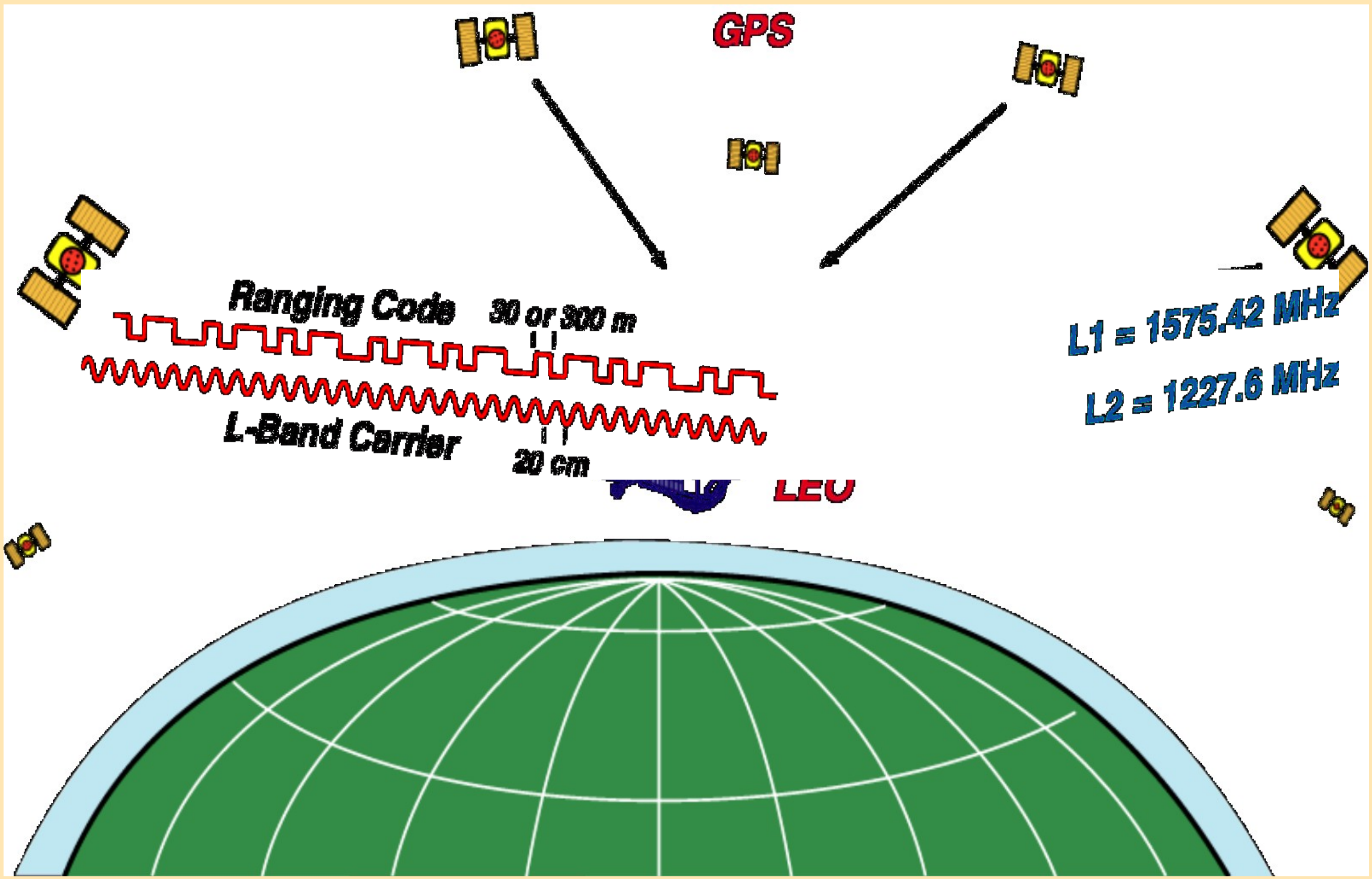

Remote Sensing with Reflected GPS

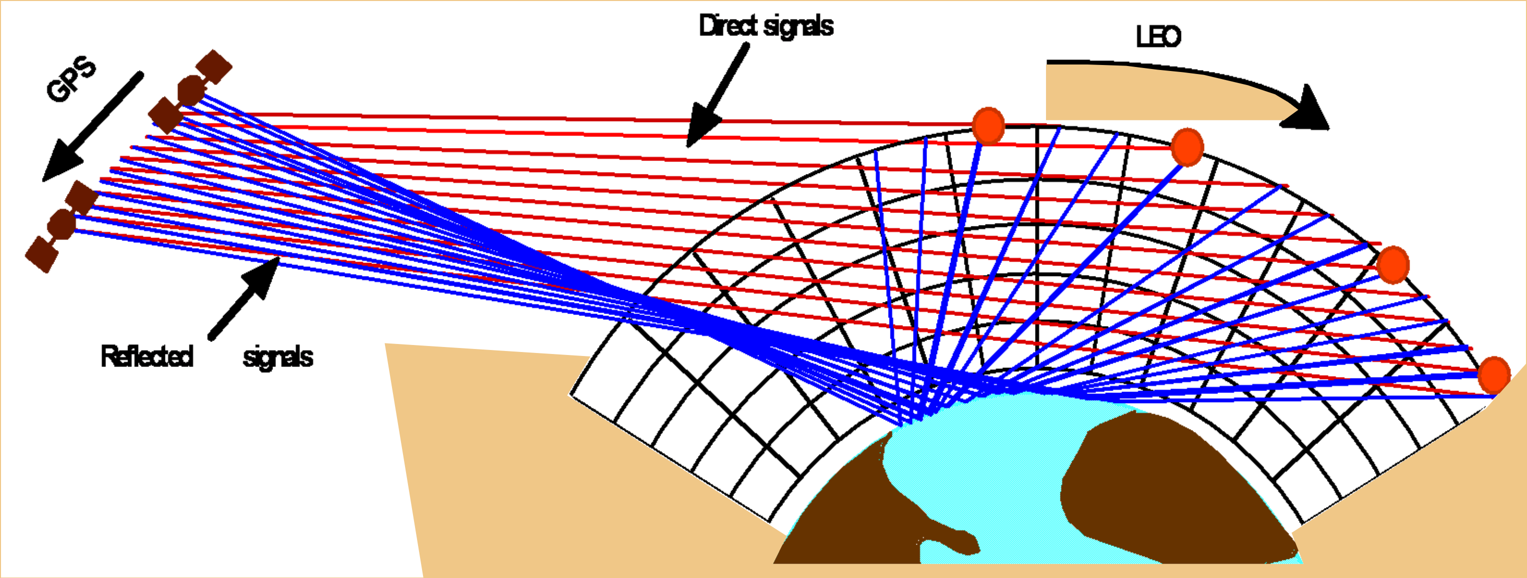

Applications

- Ocean Altimetry (topography, circulation)
- Scatterometry (sea state, surface winds)
- Atmospheric and Ionospheric Imaging

Ground-/Space- based GNSS Observations

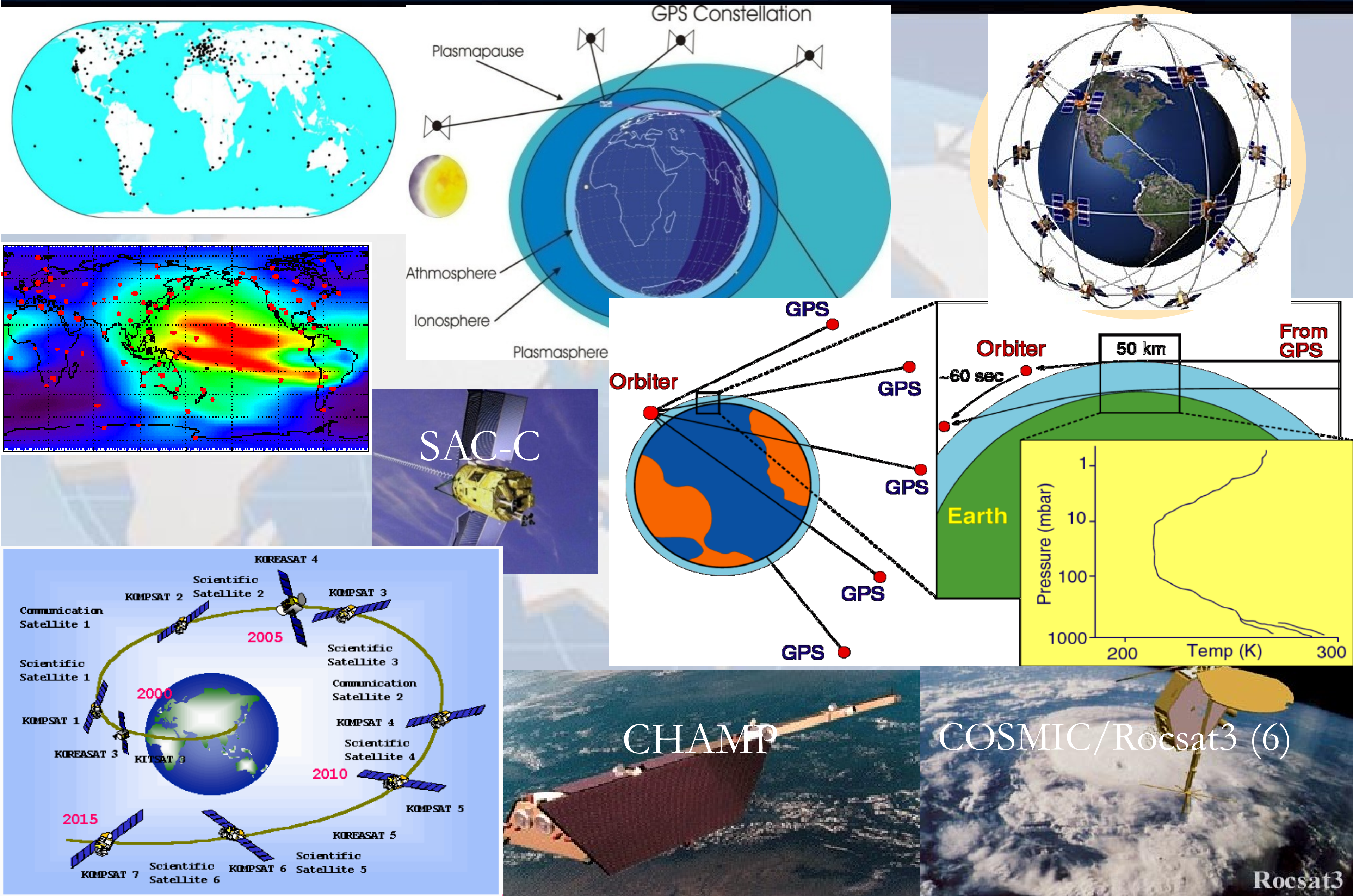

GNSS as a new remote sensing tool

- GNSS-based remote sensing for atmosphere, ionosphere, oceans, ice, soil (moisture), etc. using radio occultation and reflectometry.

- Development of technologies and know-how for future micro satellite constellations (formation flights) using GNSS.

- Passive radar for altimetry and scatterometry using a beam-steerable antenna.

- Oceanographic and hydrological applications:

  Sea level (altimetry), Ocean wave spectra (2D), roughness, swells (scatterometry), Retrieval of wind directions, Retrieval of sea ice parameters, Tsunami detection, and possible soil moisture extraction.

1) GNSS Atmospheric Sounding

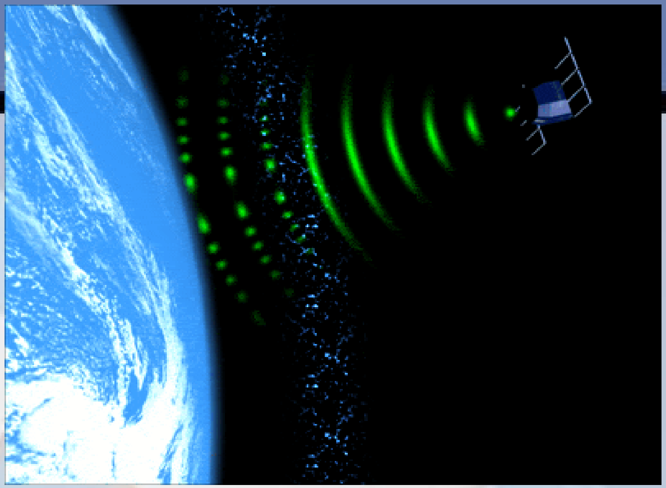

Optic and Geometry GPS Signal:

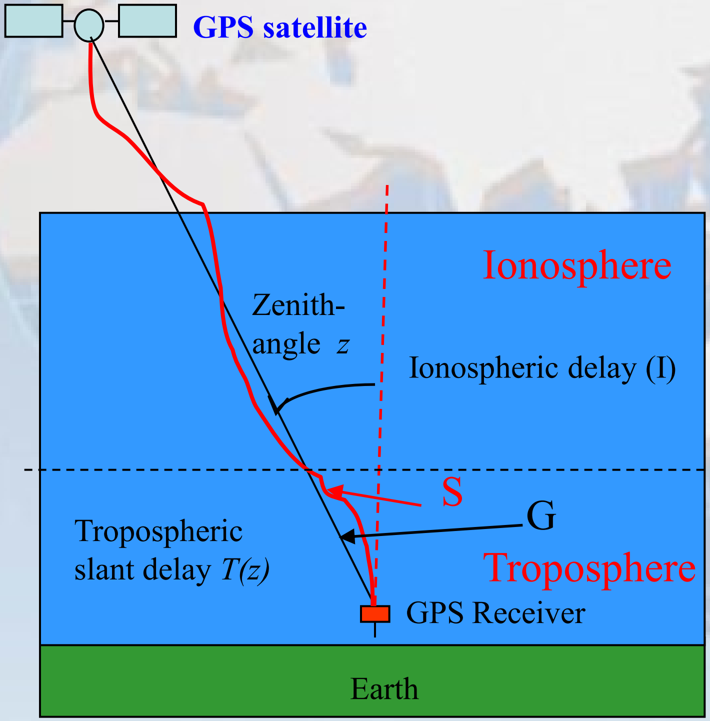

GPS Tropospheric delay & Applications

- Monitoring the precipitable water vapor (PWV) for Weather forecast and Climatologic research.
- Corrections of tropospheric delay for microwave techniques, e.g. InSAR, GPS etc.

GPS Ionospheric delay & Applications

- Correct the ionospheric error of GPS measurements (with 1-100 meters errors)
- Monitor ionospheric activities and irregularities, e.g. ionospheric scintillation, storms
- Investigate the solid-earth deformation due to coupling with the ionosphere
- **Investigate space environment effects on Earth climate**

GPS Navigation, POD and Coordinates

Subdiurnal atmospheric tides by GPS-ZTD

The atmospheric density changes the refractive index of the zenith column of air under the influence of the atmospheric tides, which causes oscillations in the ZTD at tidal frequencies. Thus, the oscillations in ZTD within periods of a solar day (diurnal) and half a solar day (semidiurnal) may reflect the diurnal and semidiurnal tides induced on the atmosphere by thermal and gravitational excitation from the Sun. Under the assumption of hydrostatic equilibrium, the change in pressure with height is related to total density at altitude h through the approximate relationship with hydrostatic equilibrium approximation as

$$\mathrm{d}p = -\rho(h)g(h)\mathrm{d}h \qquad (3)$$

where $\rho(h)$and $g(h)$ are the density and gravity at the altitude h, respectively. Disregarding the change in the acceleration of gravity g with respect to height, the zenith hydrostatic delay (ZHD) can be further deduced as (Saastamoinen 1973)

$$\mathrm{ZHD} = kp_0 \qquad (4)$$

where k is a scale factor (2.28 mm/hPa) and p_0 is the pressure at height h_0 (Davis et al. 1985), namely ZHD $= 2.28\ p_0$. The scale factor k varies less than 1% even under severe weather conditions.

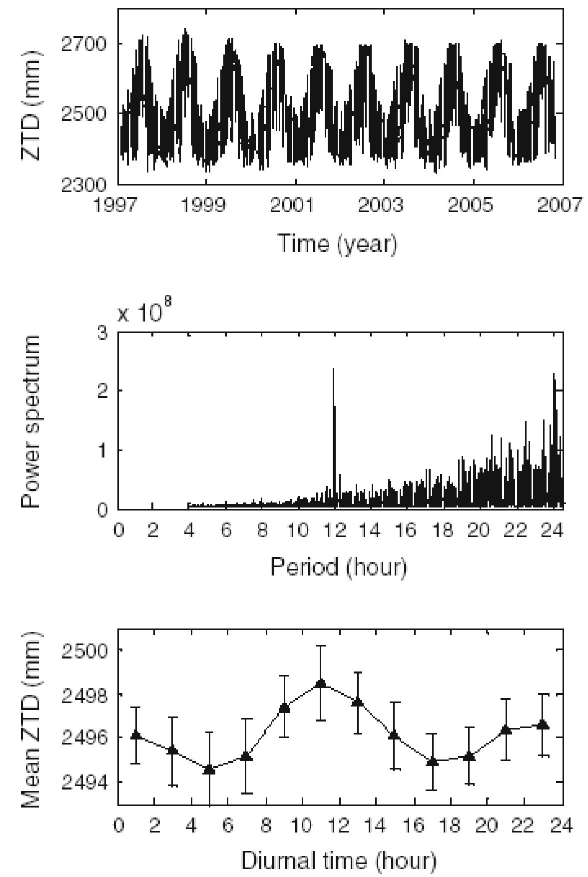

Fig. 4 Times series of zenith total delay (ZTD) (*upper*), power spectrum (*middle*) and mean diurnal ZTD values at each of local time (LT $= 1, 3, 5, \ldots, 23$) over the entire period with error bars (*bottom*) at Wuhan (WUHN), China

Jin et al. 2009, J. Geodesy

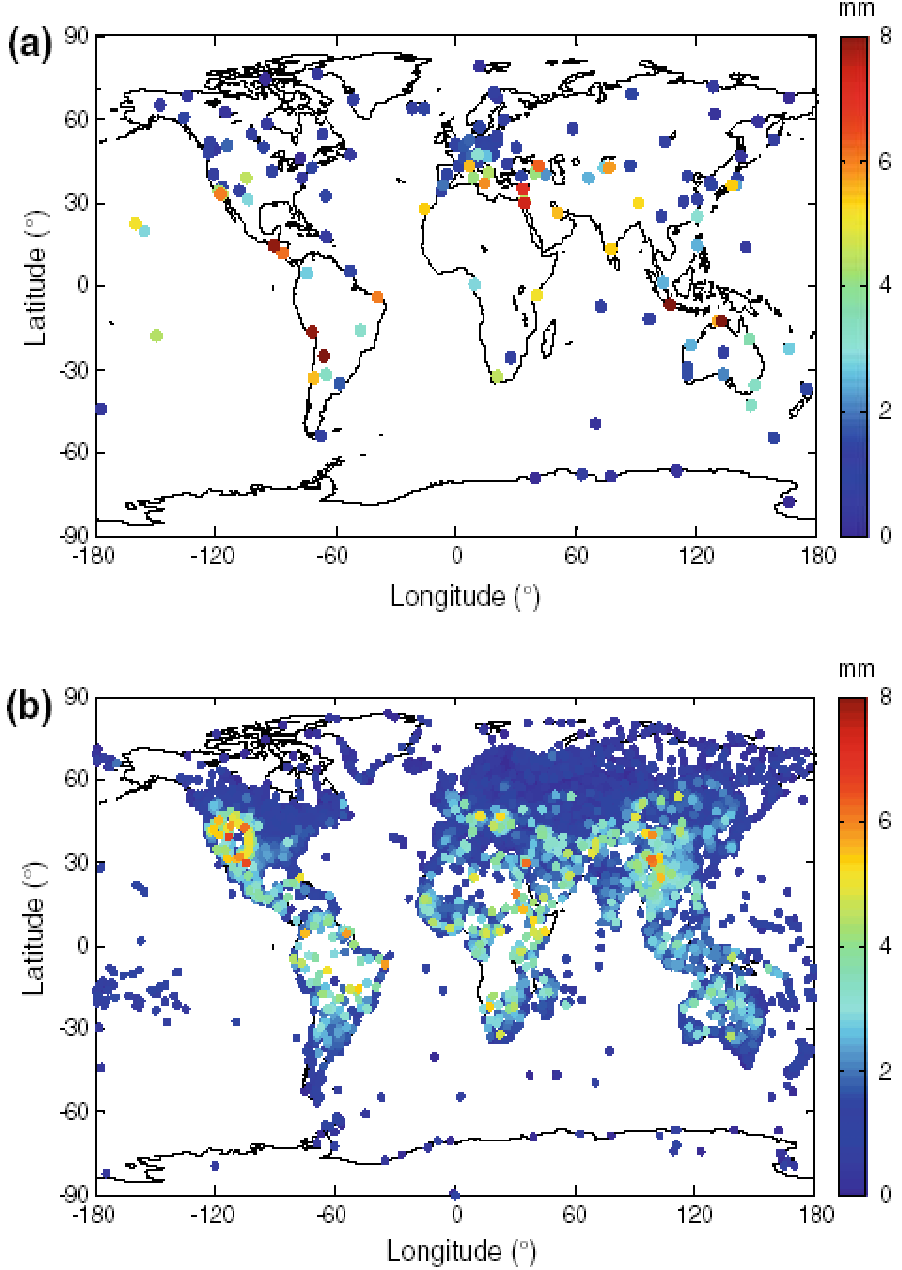

Fig. 5 Diurnal variation amplitudes (mm). **a** from GPS-derived ZTD and **b** from COADS surface pressure data adjusted by a scale factor (2.28 mm/hPa)

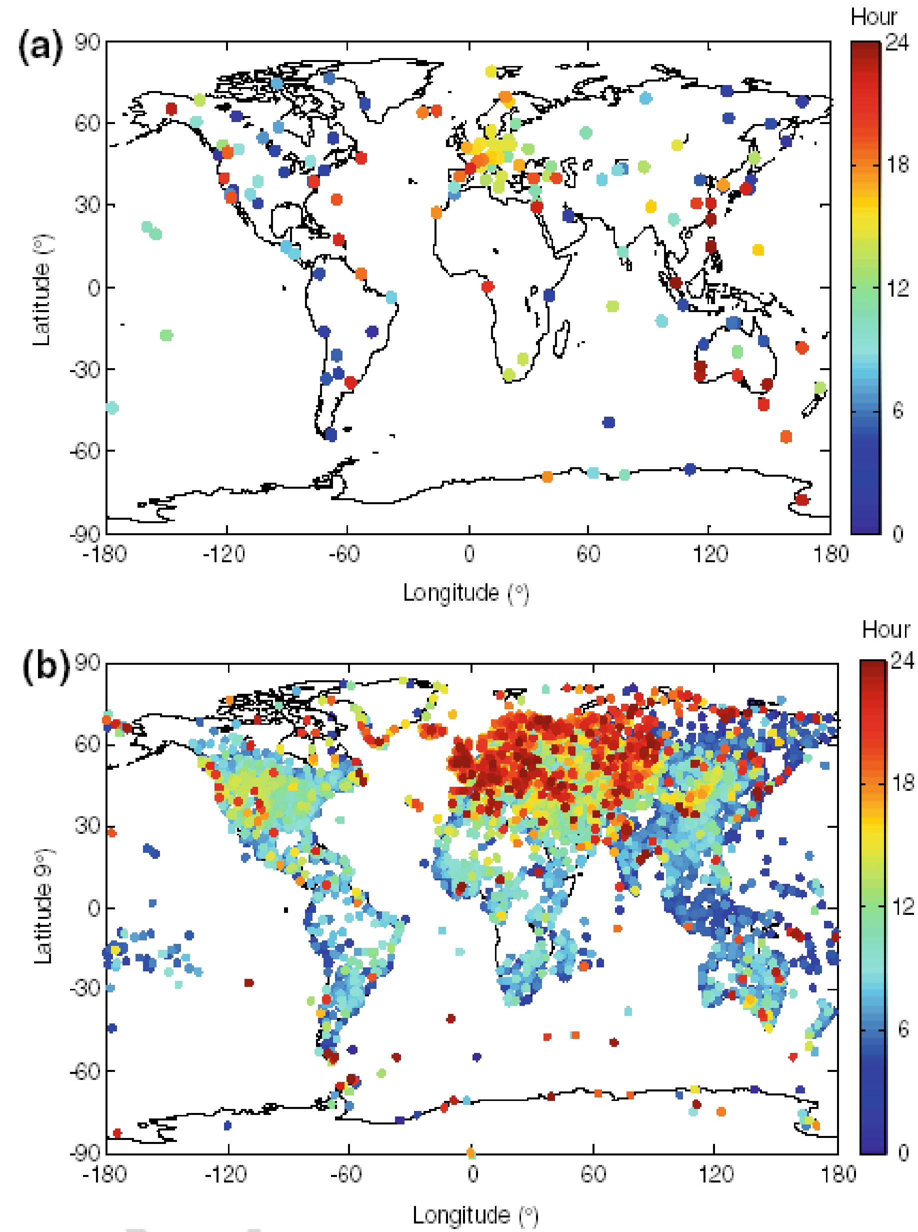

Fig. 7 Time of diurnal peak values at local time (LT: hour) where at each GPS sites longitude the Sun is at its highest elevation at 12:00 LT. **a** from global IGS GPS observations and **b** from COADS surface pressure data

Co-seismic Ionospheric Disturbance (2008 China Mw=8.0 Earthquake)

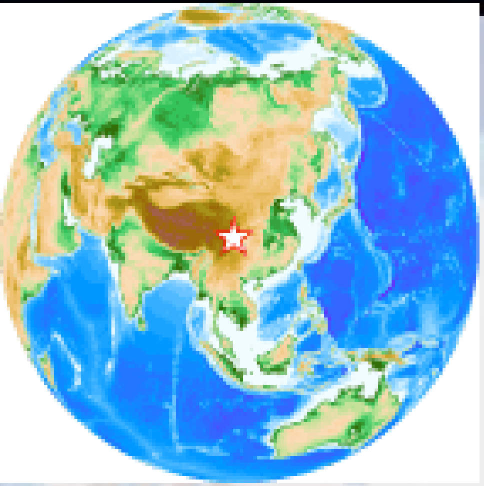

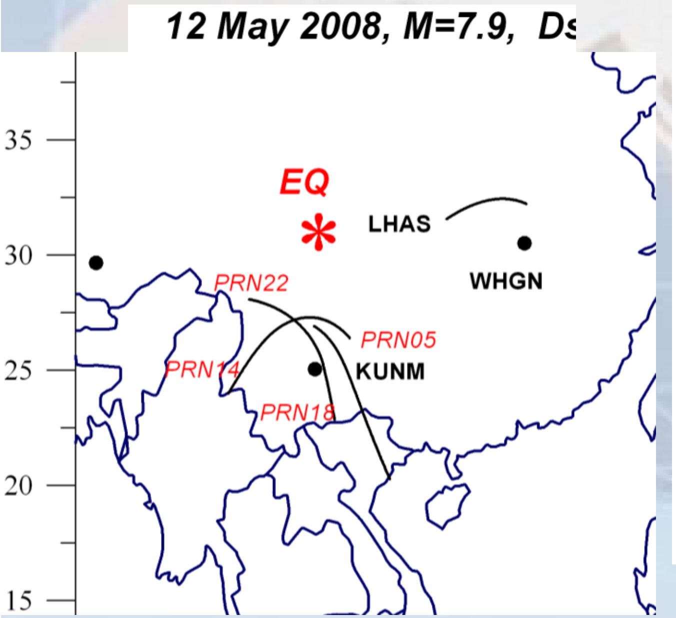

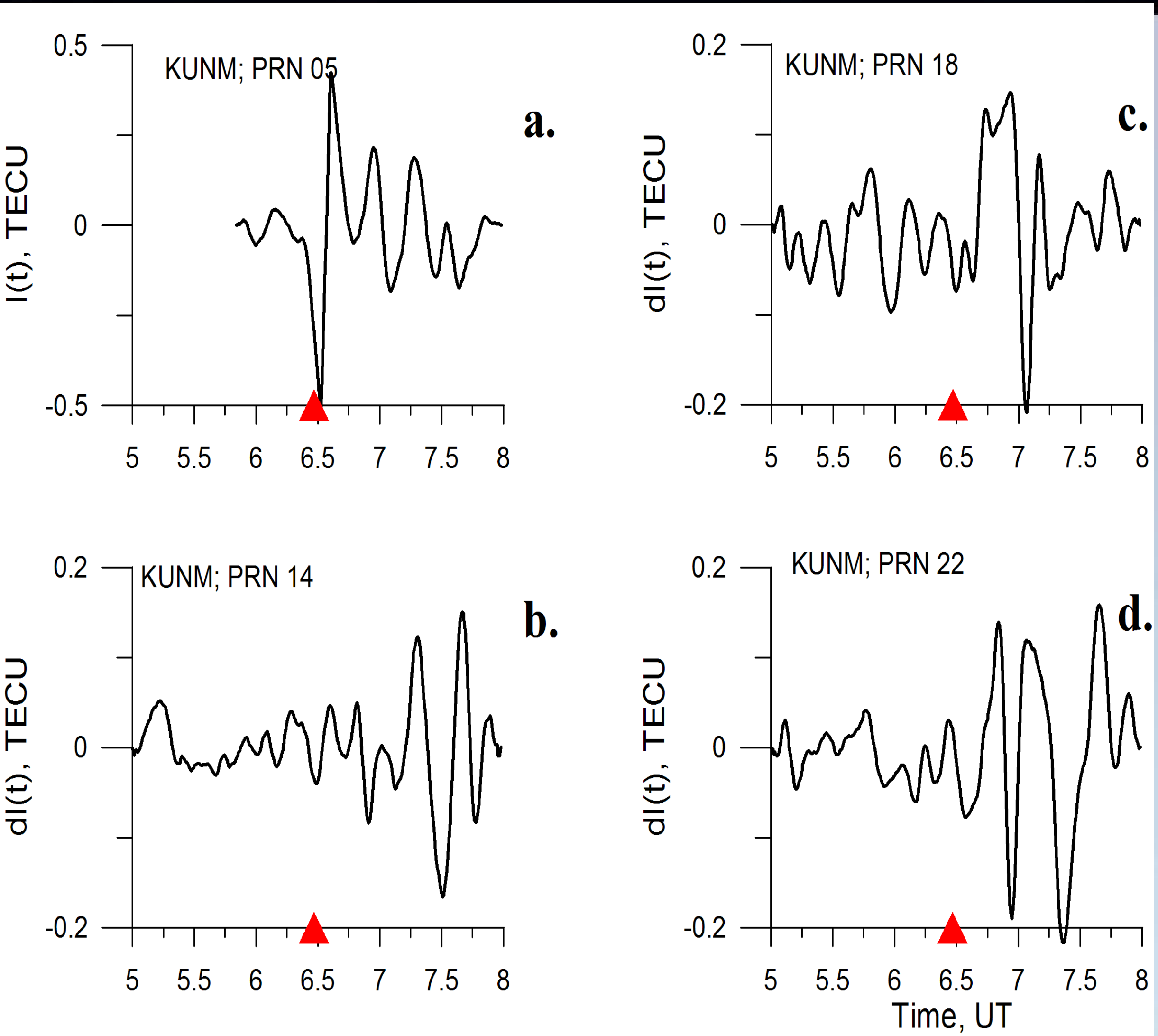

Jin, et al. 2010, Int. J. Remote Sens.

Ionospheric shock-acoustic waves

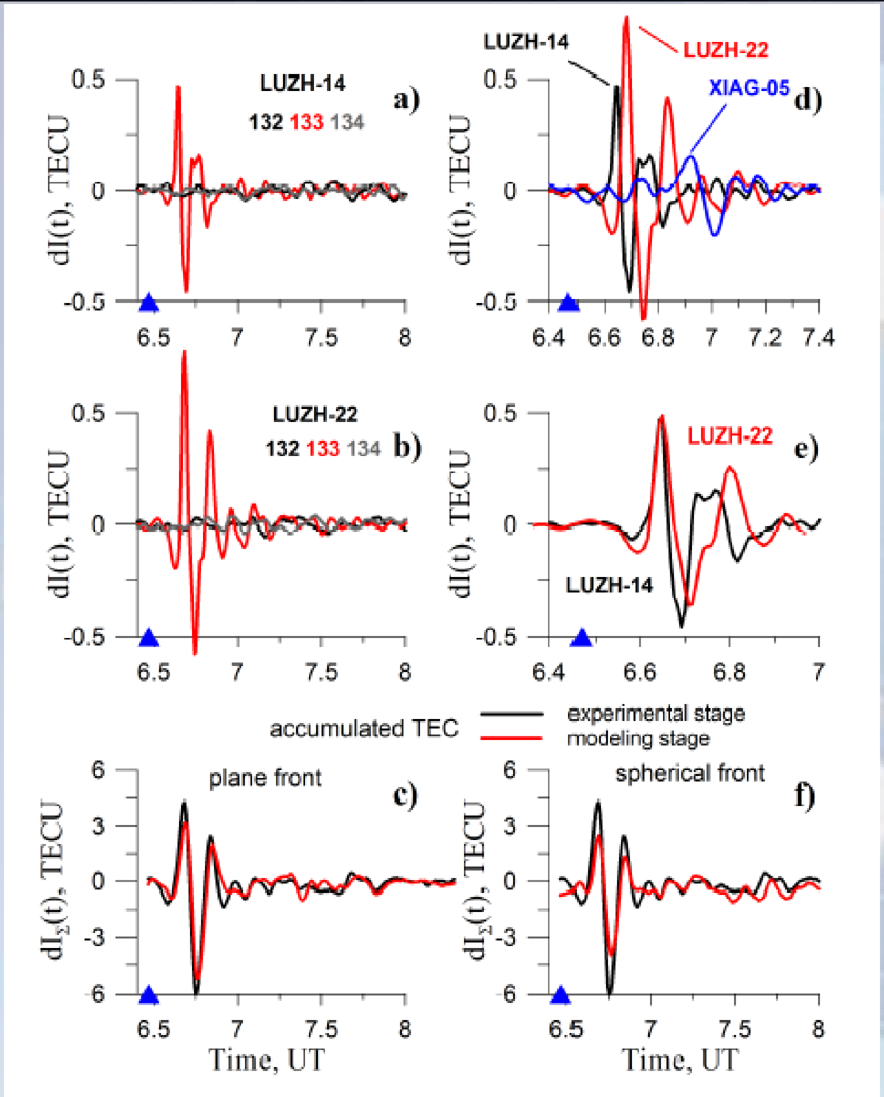

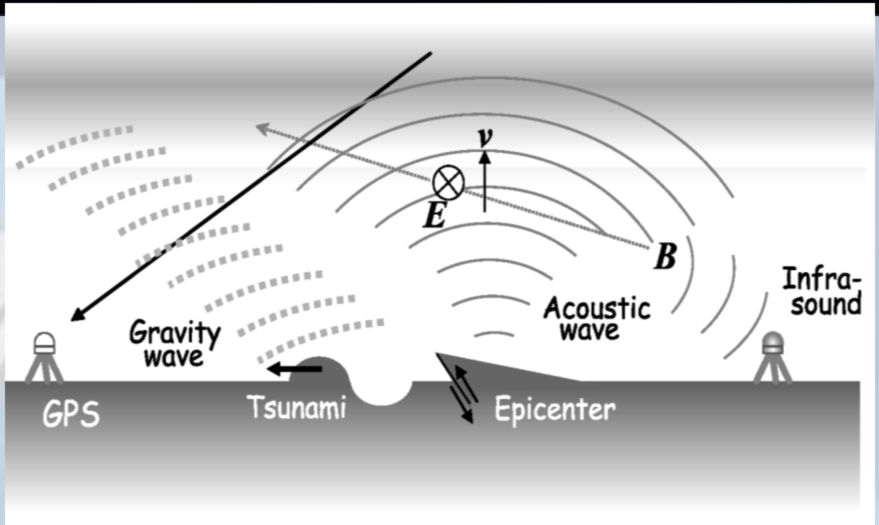

The co-seismic ionospheric disturbance at 28 GPS sites shows that an intensive N-shape shock-acoustic waves propagated north-eastward with a velocity 600 m/s, in parallel with the rupture direction.

Jin, et al. 2010, Int. J. Remote Sens.

Ground-GPS ionospheric tomography

- **Method A: Multiplicative Algebraic Reconstruction Technique (MART)**

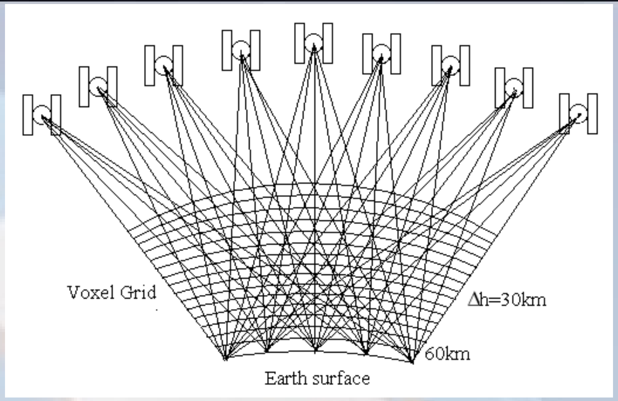

$$STEC_i = \sum_{j=1}^{M} a_{ij} n_j \qquad x_j^{k+1} = x_j^k . \left(\frac{y_i}{\langle a_i . x^k \rangle} \right)^{\lambda_k a_{ij}}$$

By iterative reconstruction with an initial guess, until the root mean square (RMS) doesn't change.

- **Method B: Singular Value Decomposition (SVD)**

$$Ax = b \qquad \boldsymbol{AXW = b} \qquad \boldsymbol{W = (AX)^{-1} b}$$

$$\boldsymbol{W} = \left(\boldsymbol{V} \left(\mathrm{diag}(1/\boldsymbol{w}) \boldsymbol{U}^T \right) \right) \boldsymbol{b}$$

⟹ **No need initial values**

Jin et al. J. Geodesy, 2009

More SVD is referred to Bhuyan et al.(2002)

Ionospheric electron density profiles over Korea by GPS measurements

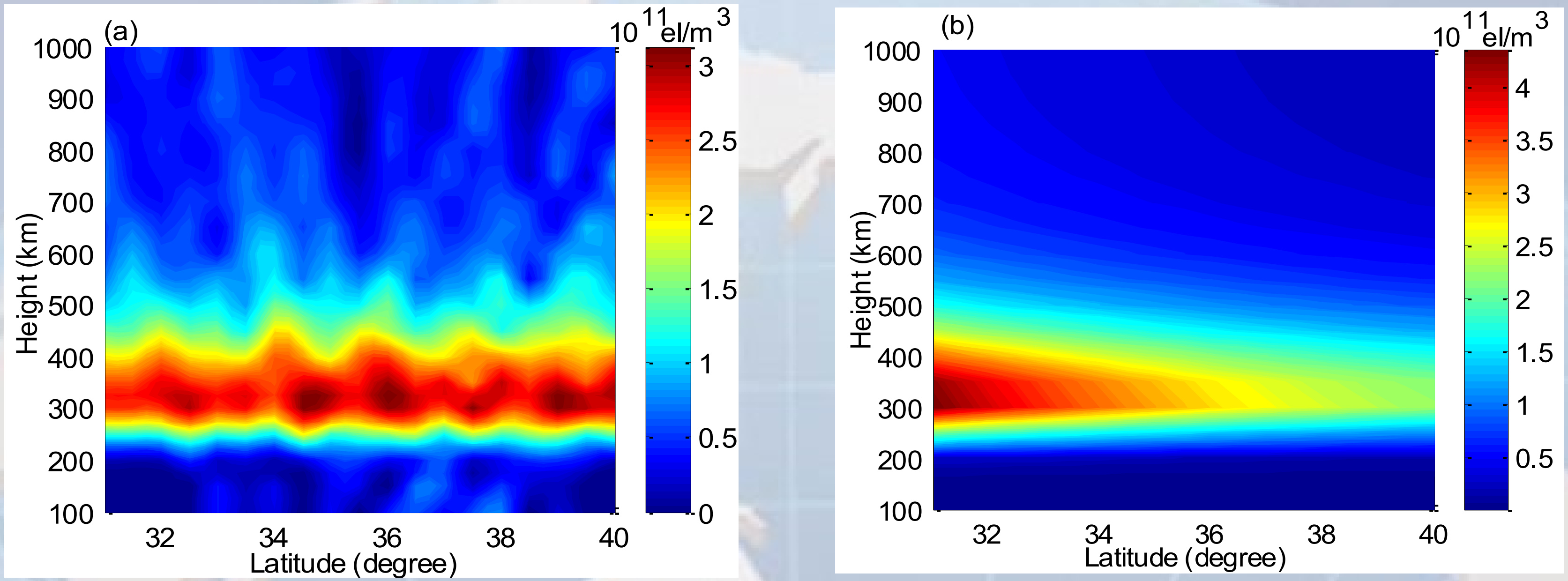

Figure 2 Ionospheric electron density distributions with the latitude of South Korea on 28 October 2003 at UT: 13:00 (LT: 22:00). (a) ground-based GPS tomography reconstruction; (b) IRI-2001.

Jin et al. J. Navigation. 2007

Ionospheric behaviors to space weather by GPS, CHAMP, and Ionosonde

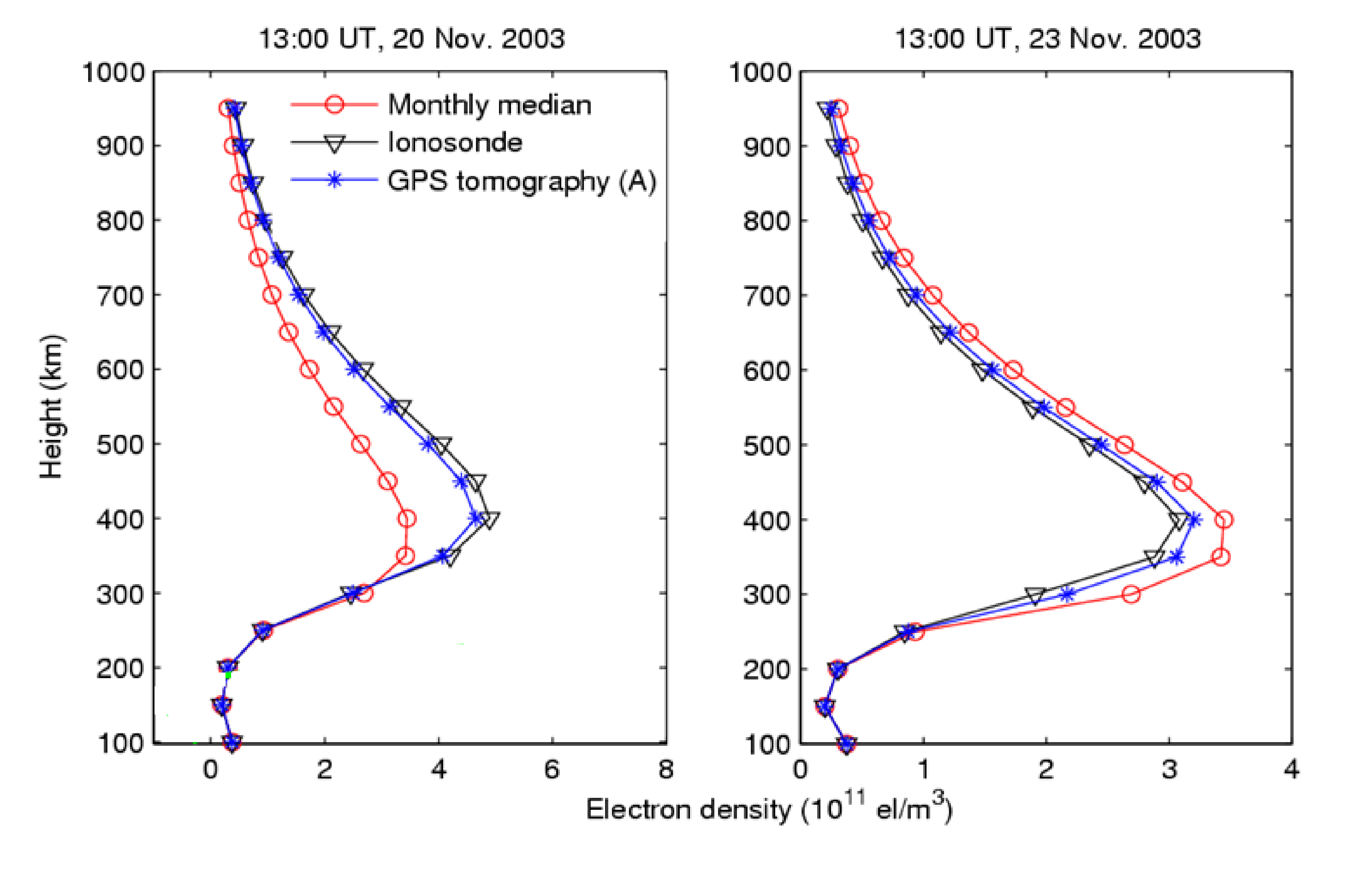

Fig. Ground-GPS, CHAMP and Ionosonde observed and one month GPS-derived average electron density profiles at 13:00 UT.

Jin et al. J. Geodesy, 2008

2) Bistatic GPS Reflections

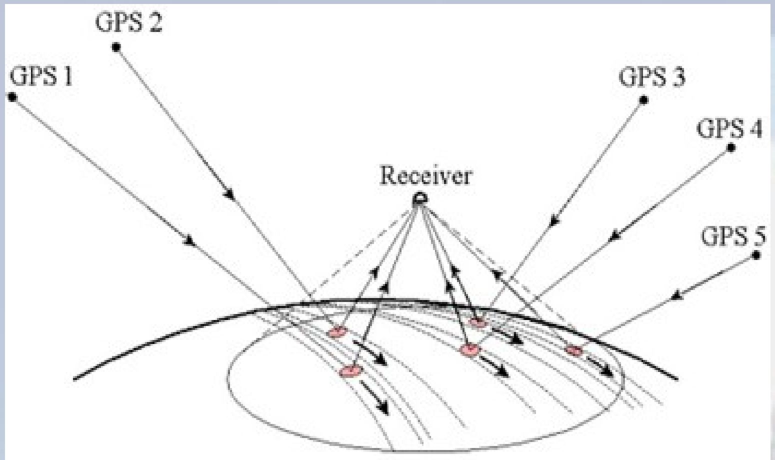

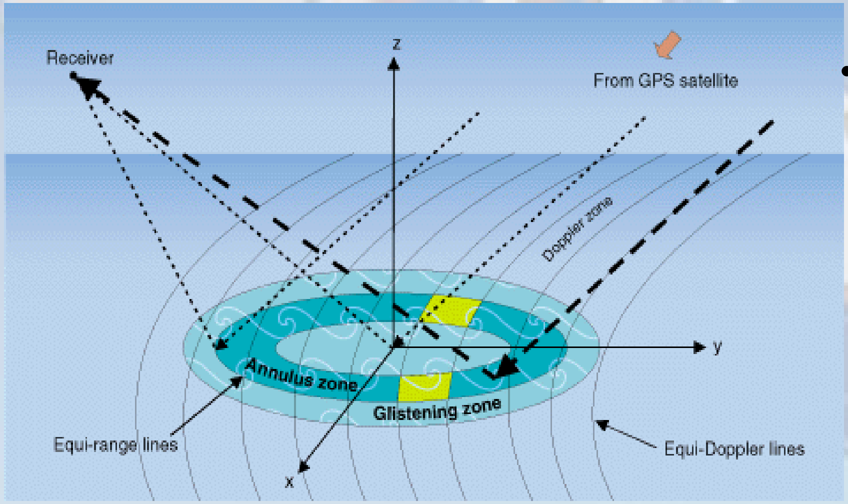

- The satellites in the GPS constellation are constantly bombarding the earth with radio signals. Part of the signal is reflected from the earth's surface back into space. The reflected signal component is very weak.
- A spacecraft placed into low earth orbit could simultaneously measure direct and reflected GPS signals, and the data could be used to deduce information about the reflecting surface (i.e., the Earth's surface and oceans).
- The signal reflection footprint on the surface of the earth is defined by the intersection of equi-range and equi-Doppler contours in what is called the glistening zone, which is centered on the specular reflection point.. A delay-doppler mapping receiver (DDMR) would be used to take measurements across the range of delay and Doppler offsets. Measurements taken at a specific Doppler and delay offset would correspond to specific regions within the glistening zone.

ICESat and GRACE
GPS Receiver Mission Support

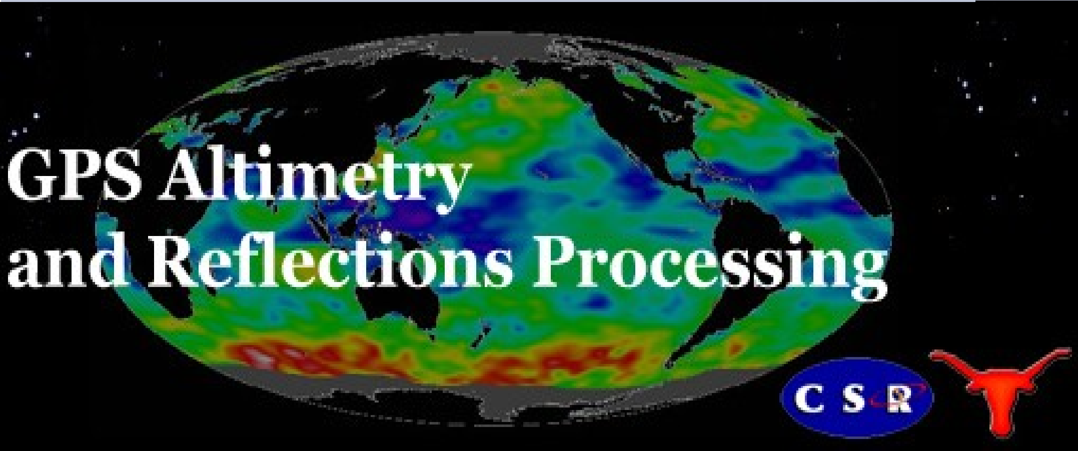

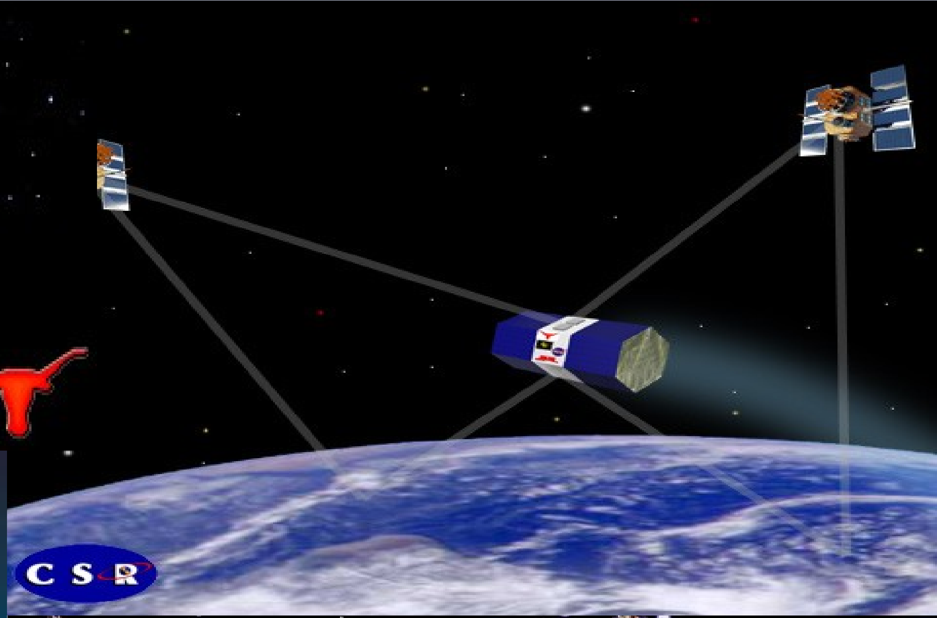

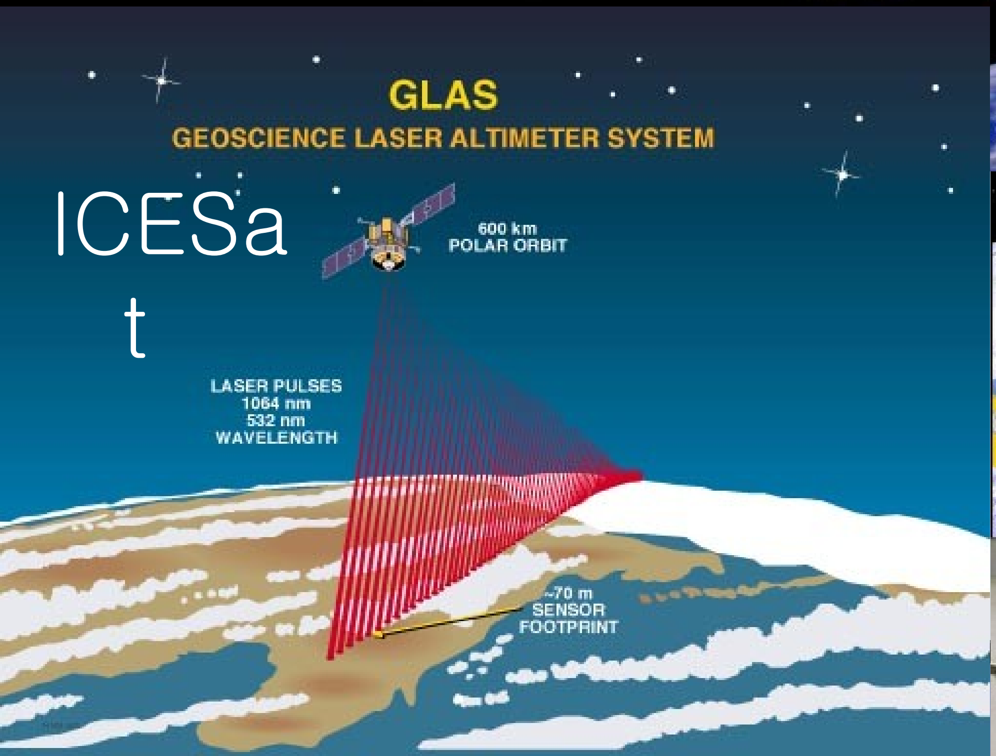

Blackjack GPS Receiver

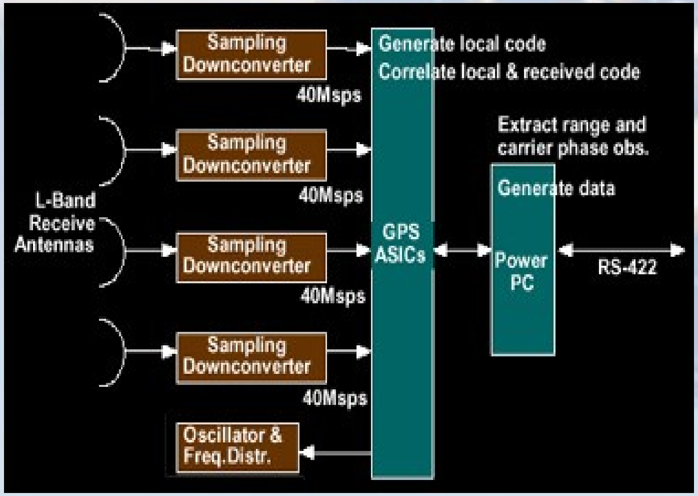

- JPL's Blackjack GPS receiver is a high-precision space-rated GPS receiver with dual-frequency tracking capabil ity. The Blackjack is an unclassified receiver, and uses a patented codeless processing technique that allows it t o utilize the P-code signal without knowledge of the enc ryption code. The Blackjack is controlled through flexi ble and versatile software implementations of various re ceiver functions. This environment is conducive to addi ng new capabilities, based on the mission requirements.
- BlackJack GPS flight receivers are being used on the fol lowing space missions: SRTM (2000), SAC-C (2000), C HAMP (2000), JASON-1 (2000/01), VCL (2000), FED Sat (2001), ICESat (2001), and GRACE (2001). ICESat and GRACE are both CSR-managed missions.
- In the Fall, CSR will acquire a Blackjack from JPL to be used in research and mission support for ICESat and GR ACE.
- More information: JPL Press Release

Disaster Monitoring Constellation (DMC) in UK

- The Disaster Monitoring Constellation (DMC) is an international program initially proposed in 1996 and led by SSTL (Surrey Satellite Technology Ltd), Surrey, UK, to construct a network of five afford able Low Earth Orbit (LEO) microsatellites. The objective is to provide a daily global imaging capabi lity at medium resolution (30-40 m), in 3-4 spectral bands, for rapid-response disaster monitoring and mitigation.

Table 1, UK DMC Data collections from Sept 04 to Sept 05 (times are approximate). All ocean collections have NDBC in-situ buoy comparisons unless otherwise noted.

	Date d/m/y	Time (UTC)	PRN	Region
R10	03/09/2004	07:25:15 AM	17	Northwest Pacific
R11	08/11/2004	07:49:80 AM	15	Northwest Pacific
R12	16/11/2004	07:54:46 AM	22	Northwest Pacific
R13	26/11/2004	07:36:36 AM	22	Northwest Pacific
R14	14/01/2005	10:23:58 AM	13	Alaska Pacific
R15	30/01/2005	09:05:21 AM	13	Hawaii
R16	30/01/2005	10:24:04 AM	13	Alaska, Ice
R18	04/03/2005	08:27:16 AM	27	Hawaii
R19	11/03/2005	07:46:09 AM	13	Northwest Pacific
R20	21/03/2005	07:29:56 AM	13	Northwest Pacific
R21	02/05/2005	09:16:11 AM	29	Hawaii
R22	17/05/2005	08:50:40 AM	26	Hawaii
R23	25/05/2005	08:50:13 AM	27	Land, N America
R24	29/05/2005	06:26:39 AM	28	Southwest Pacific
R25	03/06/2005	06:29:27 AM	31	Southwest Pacific
R27	15/06/2005	08:57:01 AM	9	Hawaii
R28	23/06/2005	11:15:30 AM	*	Antarctica, Ice
R30	24/06/2005	09:29:08 AM	5	Alaska Pacific
R31	07/07/2005	09:33:39 AM	5	Hawaii
R32	22/07/2005	09:08:07 AM	30	Hawaii
R33	24/07/2005	08:44:36 AM	5	Hawaii
R34	09/08/2005	10:21:14 AM	15	Alaska Pacific
R35	10/08/2005	07:46:07 AM	30	Northwest Pacific
R36	12/08/2005	09:07:31 AM	30	Hawaii

Gleason et al., 2007

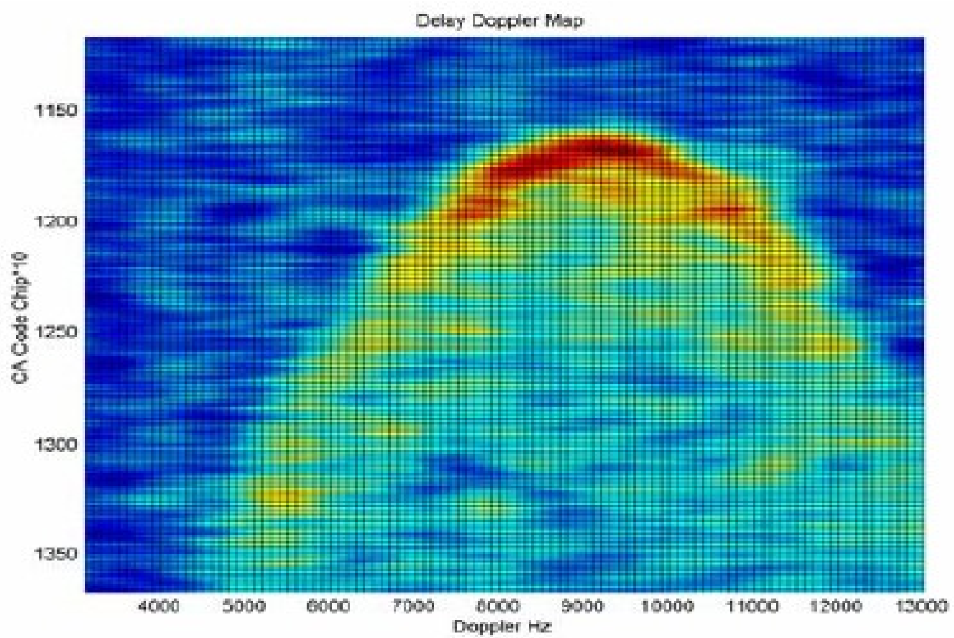

Figure 4 Delay Doppler Map, 21/03/05 (R20), wind speed 3.6 m/s, wave height 4.1 m. (Increasing power of signal represented by colours from blue to red.)

Soil moisture

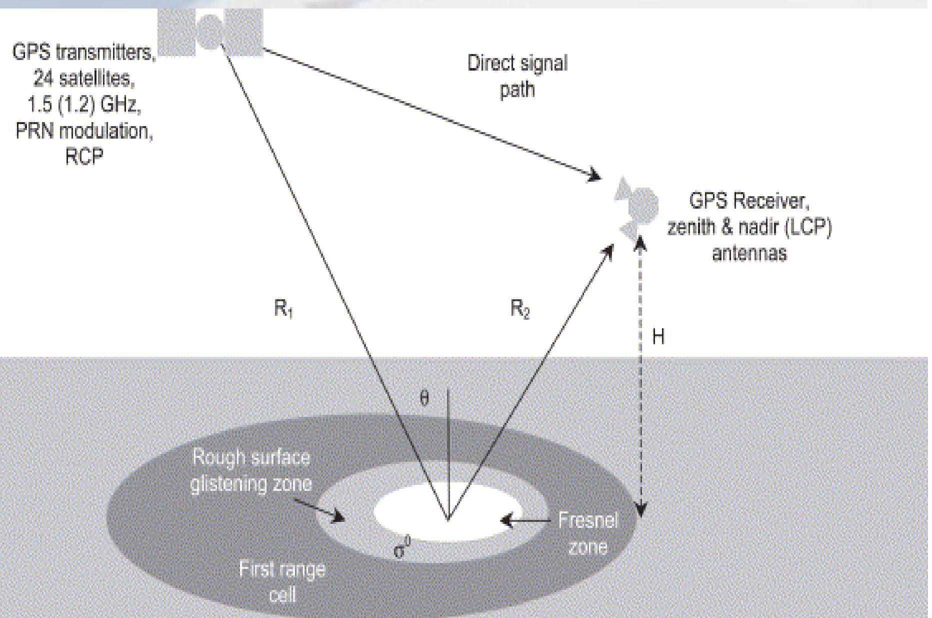

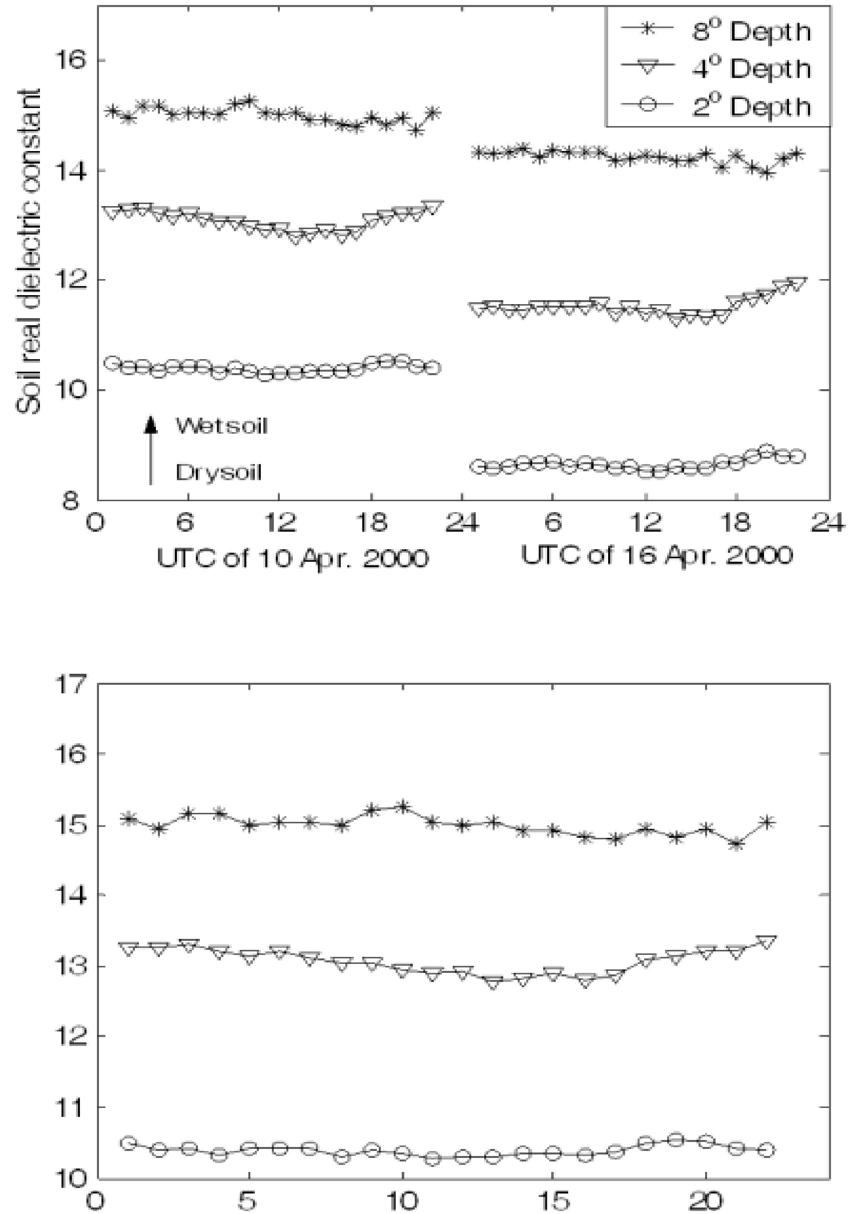

Soil moisture data from
USDA SCAN site (Masters et al., 2000.)

Soil moisture by ground GPS observations

Larson et al. (2008)

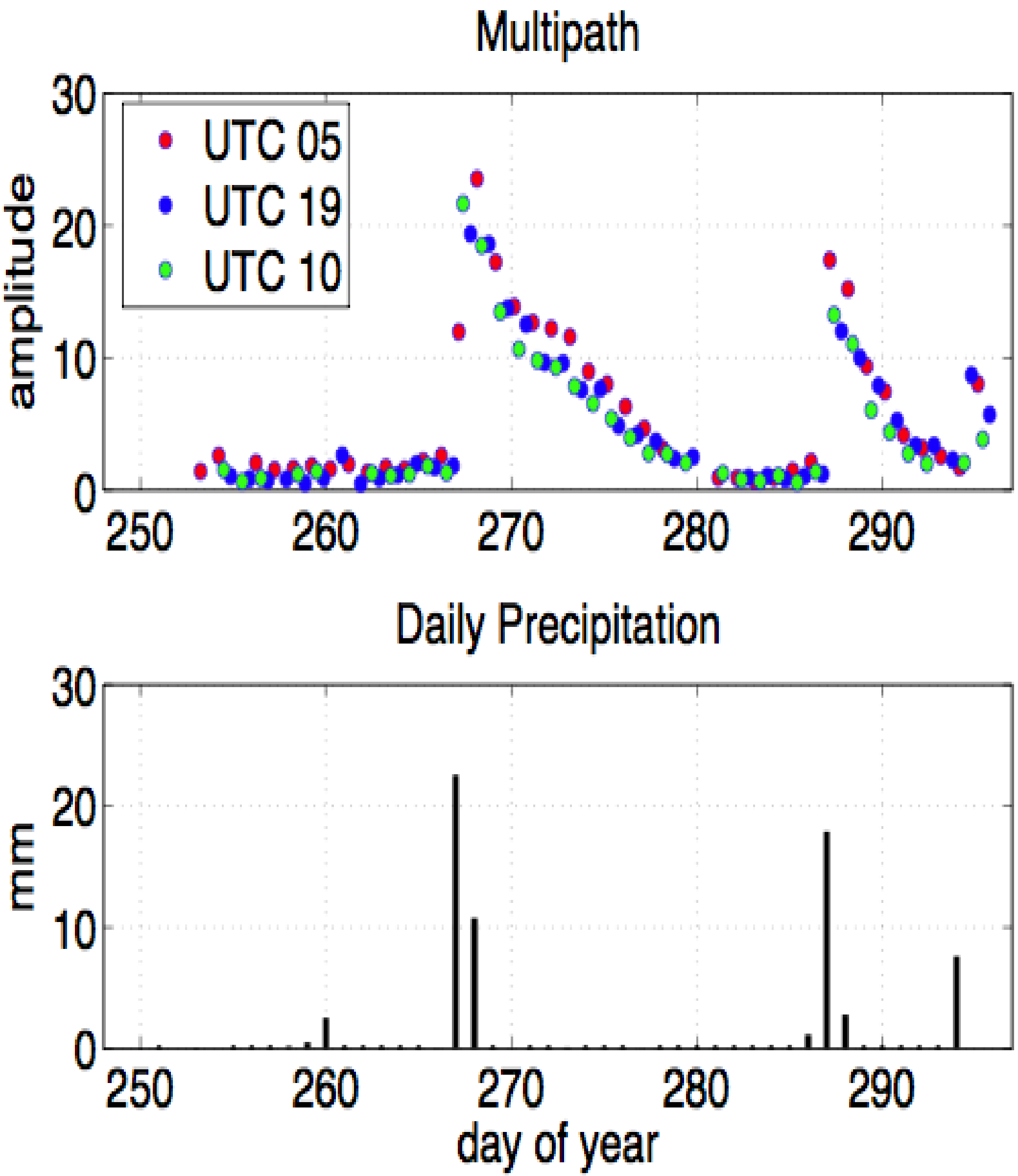

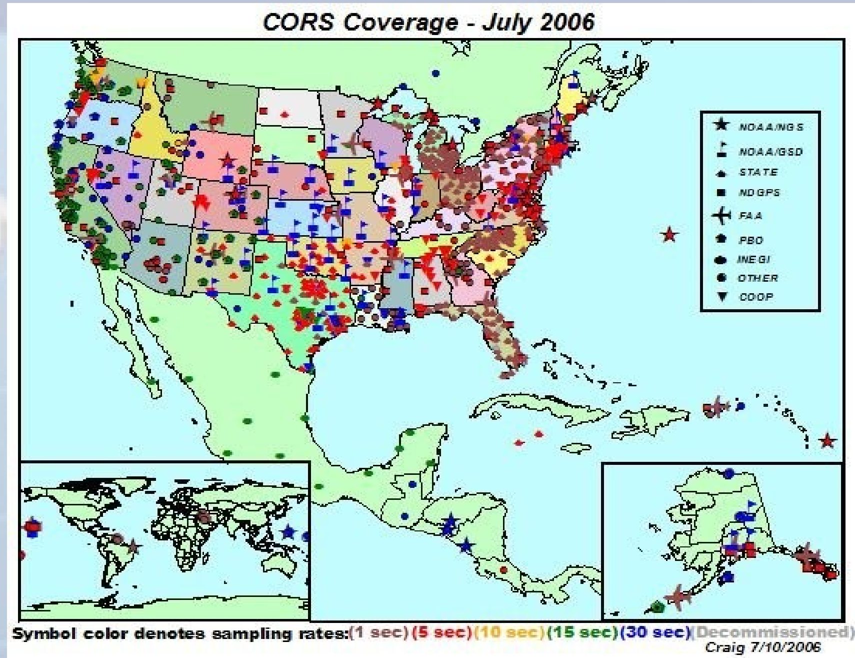

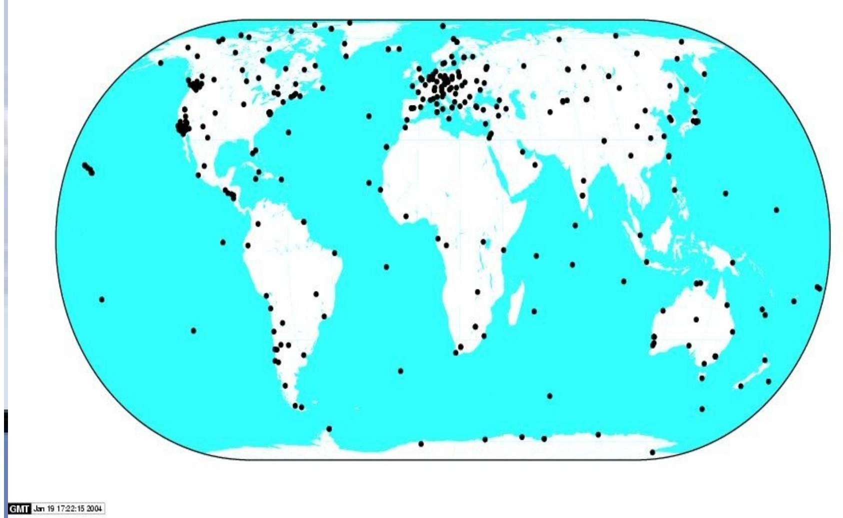

Snow/ice thickness

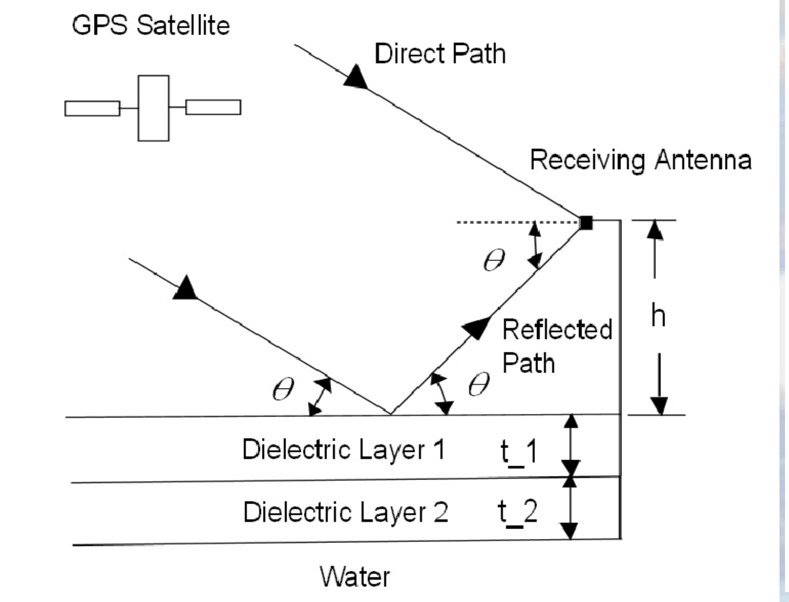

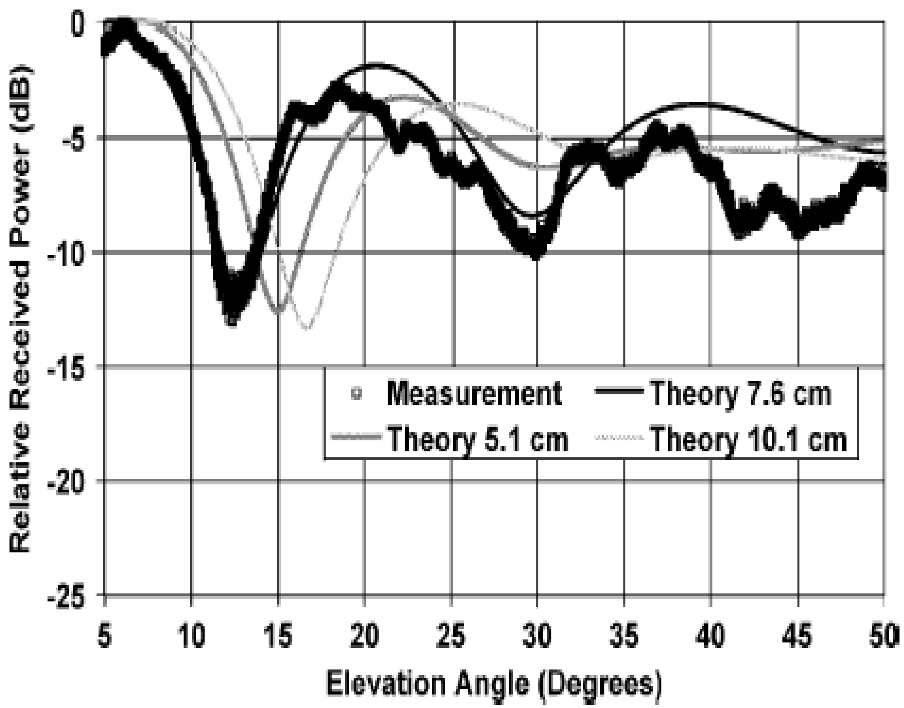

Fig. 4. (Lines) Theoretical and (square) measured elevation plots for a ground reflector covered by 5.1-, 7.6-, and 10.1-cm-thick snow layers with h = 45.1 cm. The value $\varepsilon_{\text{snow}} = 1.48 - i2.76 \times 10^{-4}$ is used in the model.

Jacobson., 2008

Hurricane Dennis with GPS-R and Dropsondes

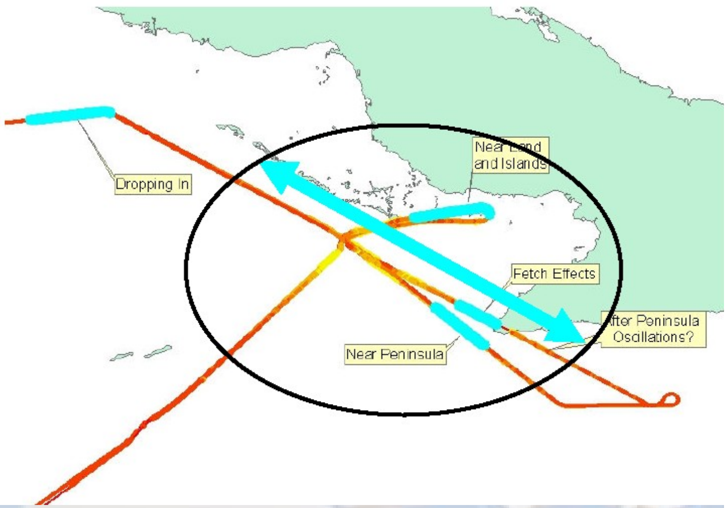

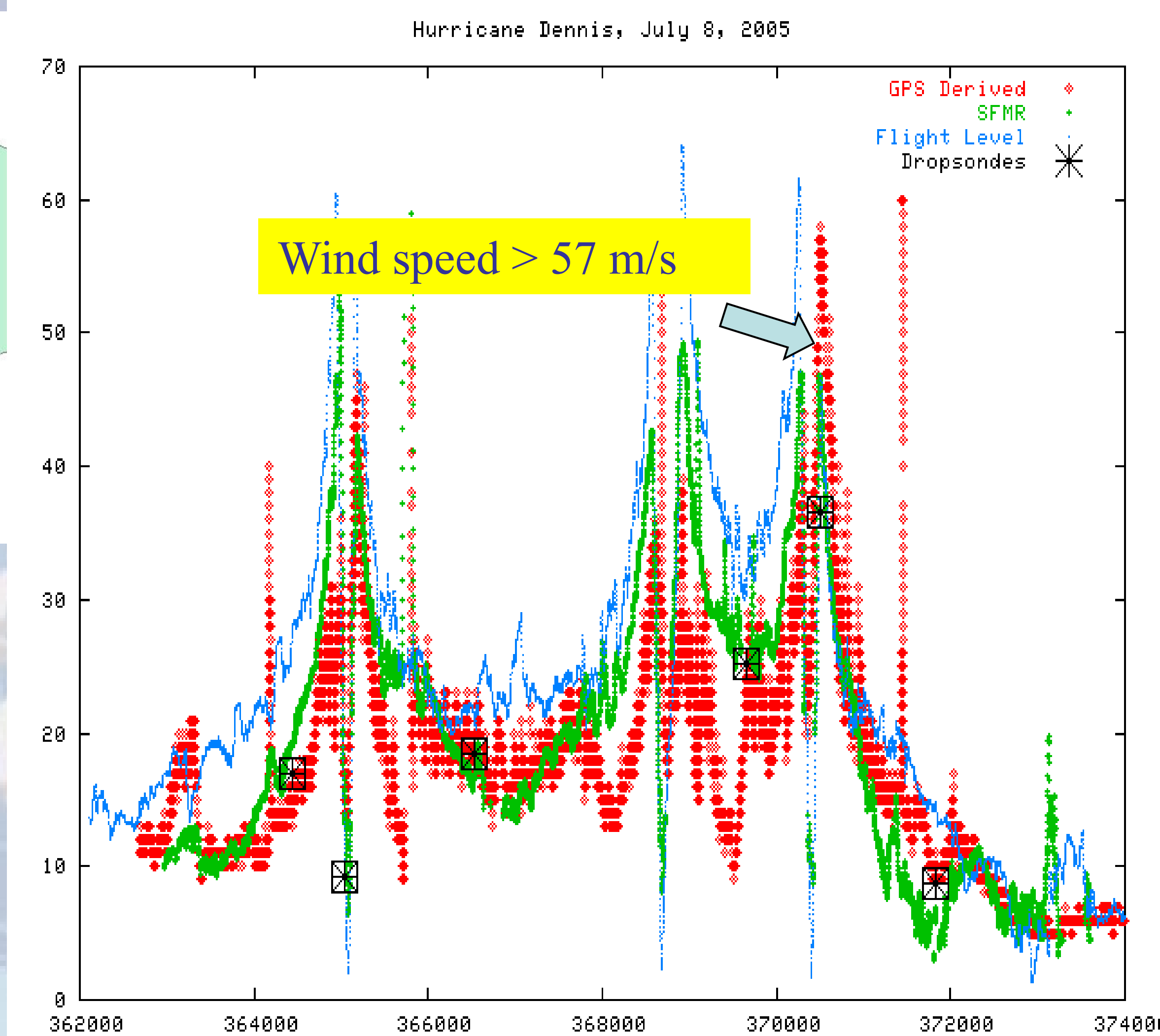

Stepped Frequency Microwave Radiometer (SFMR)

Katzberg et al., 2005

GITEWS (German Indonesian Tsunami Early Warning System)

- **GPS Reflectometry & Scatterometry Receiver Technology for future tsunami detection**
- GPS Scatterometry and Reflectometry are seen as valu able new techniques in the field of altimetry, oceanogr aphy and glaciography. The high reflectivity of GPS si gnals in the frequency range of L-Band (1,2 and 1,6 G Hz) on water as well as iced and snow covered surface s partly compensates for the low signal intensity and a llows the detection of reflected signal components.
- In the past, experiences with special Delay Mapping G PS Receivers in balloons and planes have demonstrate d, that measurements of the sea level can be achieved with an accuracy of up to 5 cm. Quite recently, the ext raction of altimetric height information of occultation events of the CHAMP mission could be proven with a sensitivity in the decimeter range.

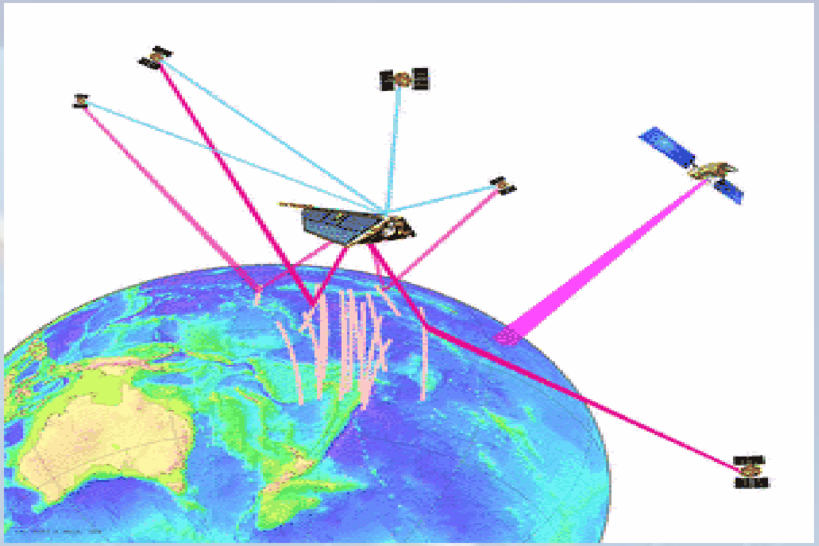

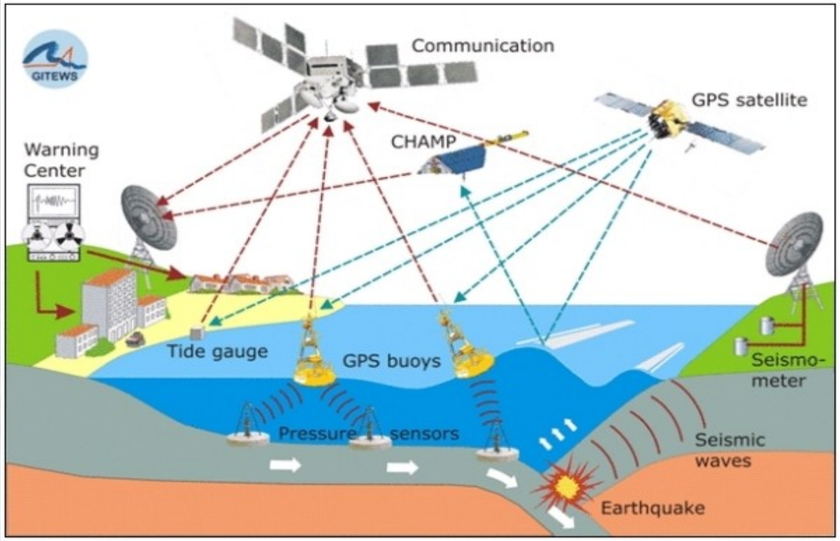

http://www.gitews.org

GNSS-RS with future more missions

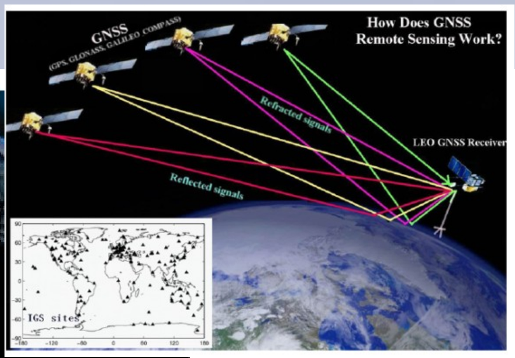

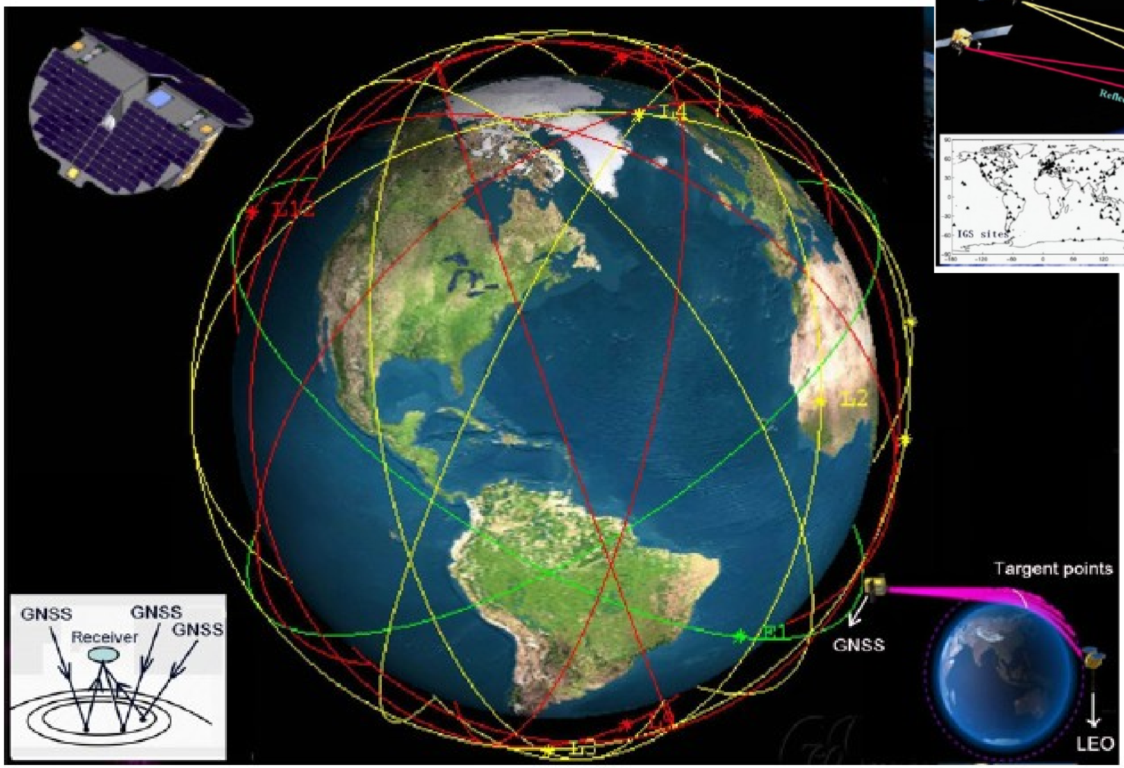

Fig. 4. CICERO (Climate Community Initiative for Continuing Earth Radio Occultation) with about 100 satellites (Yunck et al., 2007). The left lower corner shows the GNSS-Reflectometry and the right lower corner represents GNSS Radio Occultation.

GNSS Remote Sensing & Applications

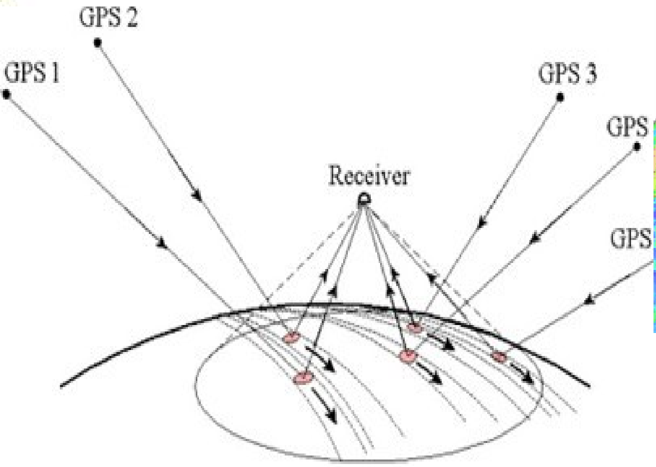

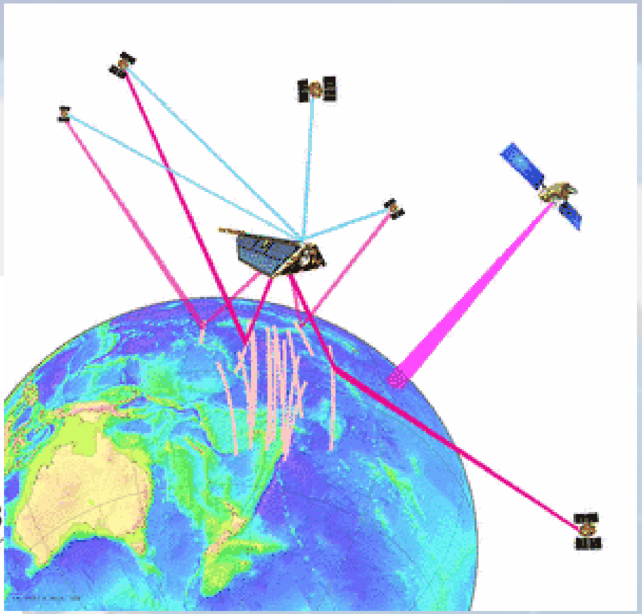

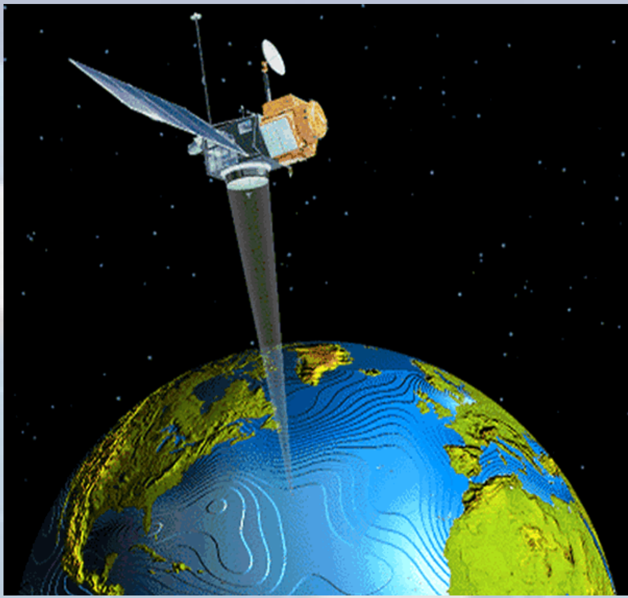

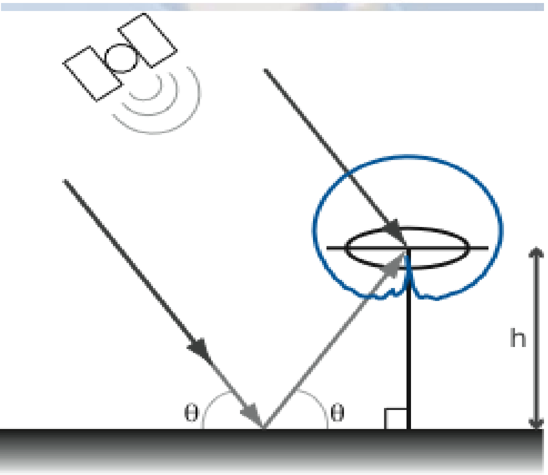

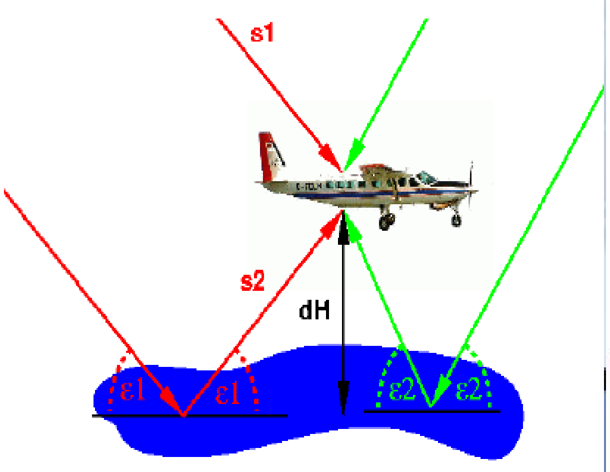

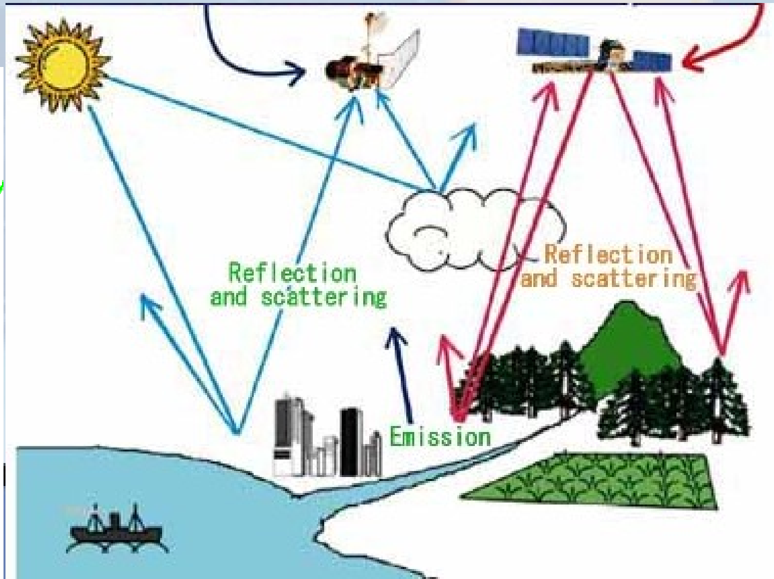

Thanks!

Shuanggen Jin
Email: sgjin@shao.ac.cn
Website: http://www.shao.ac.cn/geodesy